New Insights into the Redox Properties of Pyridinium Appended 1,2-Dithienylcyclopentenes

Lambert Sicard, Frederic Lafolet, Martial Boggio-Pasqua, Christophe Bucher, Guy Royal, Saioa Cobo

▶ **To cite this version:**

Lambert Sicard, Frederic Lafolet, Martial Boggio-Pasqua, Christophe Bucher, Guy Royal, et al.. New Insights into the Redox Properties of Pyridinium Appended 1,2-Dithienylcyclopentenes. ChemPhysChem, 2022, 23 (9), pp.e202200004. 10.1002/cphc.202200004 . hal-03675297

HAL Id: hal-03675297
https://hal.science/hal-03675297v1

Submitted on 16 Nov 2022

HAL is a multi-disciplinary open access archive for the deposit and dissemination of scientific research documents, whether they are published or not. The documents may come from teaching and research institutions in France or abroad, or from public or private research centers.

L'archive ouverte pluridisciplinaire **HAL**, est destinée au dépôt et à la diffusion de documents scientifiques de niveau recherche, publiés ou non, émanant des établissements d'enseignement et de recherche français ou étrangers, des laboratoires publics ou privés.

New insights into the redox properties of pyridinium appended 1,2-Dithienylcyclopentenes

Dr. Lambert Sicard, [a] *Dr. Frederic Lafolet,* [b] *Dr. Martial Boggio-Pasqua,* [c] *Dr. Christophe Bucher,** [d] *Prof. Guy Royal,** [a] *and Dr. Saioa Cobo** [a,e]

[a] DCM UMR 5250 CNRS and Université Grenoble Alpes, F-38000 Grenoble, France

[b] Université de Paris, ITODYS, CNRS, UMR 7086, 15 rue J-A de Baïf, F-75013 Paris

[c] LCPQ UMR 5626 CNRS and Université Toulouse III – Paul Sabatier 118 route de Narbonne, 31062 Toulouse, France

[d] Univ Lyon, Ens de Lyon, CNRS UMR 5182, Laboratoire de Chimie, F69342 Lyon, France.

[e] Institut Universitaire de France, 1 Rue Descartes, 75231 Paris

E-mail: christophe.bucher@ens-lyon.fr, guy.royal@univ-grenoble-alpes.fr, saioa.cobo@univ-grenoble-alpes.fr

Keywords. Dithienylethene, photochromism, electrochemistry, DFT calculations.

Abstract. The optical and redox properties of a methyl pyridinium appended 1,2-dithienylethene photochromic derivative have been thoroughly investigated. A complex multi-step photo/redox mechanism is proposed for the closed isomer on the ground of spectro-electrochemical and theoretical data. The generated compounds are not stable over the time because of chemical reactions associated to the redox processes and a new dithienylethene derivative incorporating a seven-membered ring has been isolated and characterized.

Introduction. Photochromic compounds have been extensively used over the past few decades as key building elements for the development of functional photo-responsive molecular materials and devices.[1–3] Diarylethene derivatives are particularly relevant for such applications due to their ability to undergo fully reversible light-induced interconversions between an "open" form, featuring two virtually isolated aryl subunits, and a highly aromatic and rigid "closed" form. These photoisomerization processes can be achieved by irradiation at specific wavelengths (UV light for the open→closed isomerization and visible light for the back transformation) or under the effect of electrical stimulations.[4–11] The fast and reversible photoisomerization of diarylethenes has already been achieved both in solution and at the solid state with very high fatigue resistance and using irradiation wavelengths which can easily be tuned by chemical functionalization.[4–6,12–14]

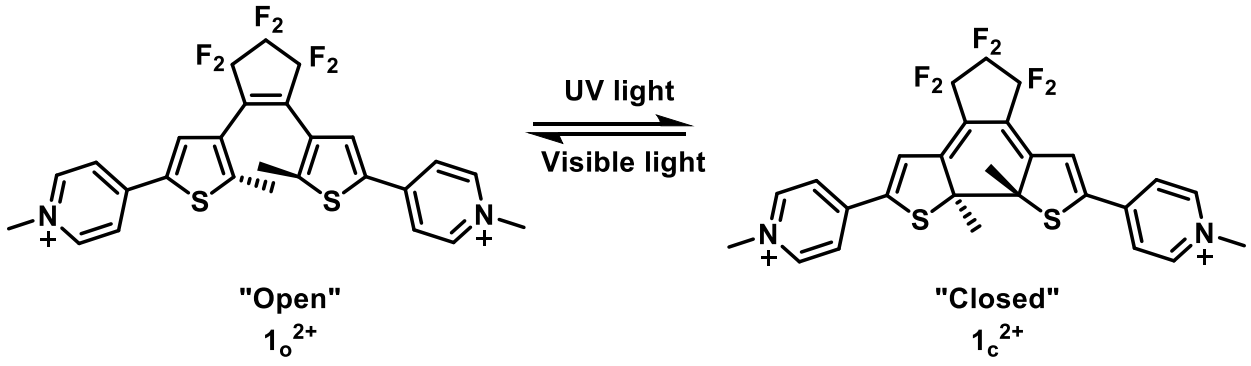

Scheme 1. Schematic representation of the photochemical isomerization of $\mathbf{1}^{2+}$.

Several studies have been specifically focused on the ring-opening[15–18], ring-closing[19–22] or on the interconversion of dithienylethene (DTE) derivatives triggered by electrical inputs[23]. Similar redox-triggered isomerization processes have also been reported for a series of dithiazolylethenes[11,14] and dithienylethenes[24,25] derivatives bearing pyridinium units. In all these reports, however, the underlying mechanisms, involving coupled electrochemical and chemical steps, were never thoroughly elucidated and therefore still remain unclear.

One key issue which remains to be addressed is the number of electrons involved in the redox processes centered on pyridinium DTE derivatives. As an example, Lehn[26] and Branda[13] have established that the one-electron electrochemical reduction of the open isomer $\mathbf{1_o^{2+}}$ triggers a cascade of events yielding, after reoxidation, the closed isomer $\mathbf{1_c^{2+}}$ (Scheme 1).[24] Further investigations carried out on DTE analogs (dithiazolylethenes) conversely suggested that the addition of two electrons *per* DTE molecule is required to achieve such isomerization.[14,25] The only conclusion that can be drawn from these previous contributions is that the number of electrons involved in the electrochemical reduction of DTEs strongly depends on the type of skeleton and on its substitution pattern.

The lack of knowledge on this key redox processes, of fundamental importance for the development of redox-responsive molecular materials, led us to take a fresh look at these issues and to carry out in-depth studies on the electrochemical response of the dithienyl-pyridinium dication $\mathbf{1_c^{2+}}$. Our contribution to the understanding of the redox processes involved in the electrochemical reduction of this molecule relies on electrochemical and spectroelectrochemical studies supported by theoretical calculations.

Materials and method

4,4'-(4,4'-(perfluorocyclopent-1-ene-1,2-diyl)bis(5-methylthiophene-4,2-diyl))dipyridinium was synthetized as previously described.[24] Electrochemical measurements were conducted at room temperature under an inert atmosphere (glove box) in a standard one-compartment, three-electrodes electrochemical cell using a Bio-logic SP300 potentiostat. All studies were carried out in anhydrous CH_3CN containing tetra-*n*-butylammonium perchlorate (0.1 M) as supporting electrolyte. CH instrument® vitreous carbon (Ø=3 mm) working electrodes were polished with

diamond paste before each recording. A CH instrument® Ag^+ electrode (0.01 M $AgNO_3$, 0.1 M TBAP, CH_3CN)/Ag was used as a reference. A platinum wire was used as the counter electrode. The reference electrode was calibrated with respect to the formal potential of the Ferrocenium/Ferrocene (Fc^+/Fc) couple in CH_3CN. Exhaustive electrolysis was carried using a large piece of vitreous carbon (2 cm^2) as working electrode. The auxiliary electrode was a Pt wire dipped in CH_3CN + 0.1 M TBAP. UV/Vis. Spectroelectrochemical measurements were carried out with a Zeiss® MCS 501 UV-NIR spectrophotometer spectrophotometer equipped with an automatic shutter. An all quartz UV-Vis immersion probe (Hellma®, 1 mm) was introduced in the electrochemical cell. The light source used for irradiation was a hand UV-lamp, 366 nm (Herolab, 7W).

EPR spectra were recorded at 100 K on a EMX Bruker spectrometer equipped with a X-band ER4102ST Bruker cavity. Aliquot of each investigated compounds were taken out of the glove box and frozen in liquid nitrogen before insertion in the cavity of the spectrometer.

Density functional theory (DFT) calculations were carried out to optimize the geometry of $\mathbf{1}^{2+}$ and of its corresponding reduced species $\mathbf{1}^{+\bullet}$ and **1**. These calculations were conducted in acetonitrile using the polarizable continuum model (PCM). Optimizations were carried out for the open- and closed-ring isomers and for selected/relevant transition states. Harmonic frequency analyses were conducted on the optimized structures to verify the nature of the stationary points (minima or transition states) on the potential energy surface and to compute Gibb's free energies of reaction (ΔG_r). Open-shell singlet (diradical) species were computed using broken-symmetry DFT calculations. To account for the spin contamination, the spin-projected energy was computed with an approximate spin-correction procedure proposed by Yamaguchi and coworkers.[27,28] Gibb's

free energies for these open-shell singlet species were computed by using the spin-projected energy. Geometry optimizations were carried out with the ωB97X-D functional[29] and the 6-31G(d) basis set. [30,31] UV-vis absorption spectra were simulated at the time-dependent DFT (TD-DFT) level using the PBE0 functional[32] along with the 6-31+G(d) basis set.[33] This combination of levels of theory using ωB97X-D for geometry optimizations and TD-PBE0 with Pople's double-ζ quality basis sets for absorption spectra calculations has proved efficient in related studies of diarylethenes.[34] All absorption spectra were computed using linear response PCM to take into account acetonitrile as a solvent. The convoluted spectra were obtained using a phenomenological Gaussian broadening characterized by a half-width at half-height of 2000 cm^{-1} for each vertical transition. All calculations were performed with the Gaussian 09 series of programs.[35]

Results and discussion

Synthesis, absorption and electrochemical experiments

$\mathbf{1_o}(PF_6)_2$ was synthetized following a previously reported procedure.[24] The UV-vis absorption spectrum of $\mathbf{1_o}(PF_6)_2$ recorded in CH_3CN displays specific signals for each isomer (Figure 1). The spectrum recorded for a 0.1 mM solution of the colorless open isomer $\mathbf{1_o^{2+}}$ exhibits one absorption band centered at 356 nm, while the closed isomer $\mathbf{1_c^{2+}}$, generated *in situ* upon submitting a solution of $\mathbf{1_o^{2+}}$ to UV light (λ = 366 nm), absorbs at 426 nm and 669 nm (dark blue solution). The simulated spectra of these two isomers (Figures S1 and S2), calculated at the TD-DFT level, show similar features. The intense absorption band observed at λ_{max} = 359 nm in the spectrum of $\mathbf{1_o^{2+}}$ is dominated by a HOMO→LUMO transition (Figure S1). The absorption maxima calculated for $\mathbf{1_c^{2+}}$ (λ_{max} = 445 nm and 685 nm) was found to be only slightly red-shifted compared to the experimental values. These computational analyses allowed us to attribute the absorption bands

observed at λ_{max} = 445 and 685 nm to the HOMO-1→LUMO and HOMO→LUMO transitions, respectively (Figure S2).

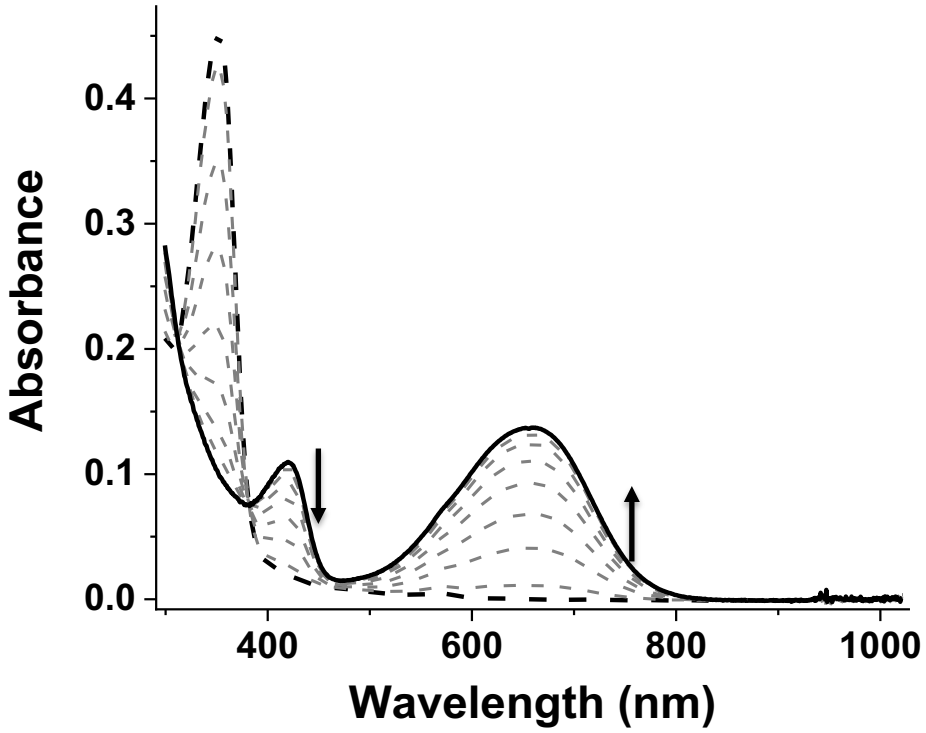

Figure 1. UV-vis spectra recorded over time upon submitting a solution of $\mathbf{1_o}^{2+}$ in CH_3CN (l = 10 mm, [c] = 0.1 mM, black dashed line) to a continuous photoirradiation (λ_{max} = 366 nm) until reaching the photostationary state (solid line).

The cyclic voltammetry (CV) curves obtained for the open ($\mathbf{1_o}^{2+}$) and closed ($\mathbf{1_c}^{2+}$) isomers are shown in Figure 2. The CV curve of $\mathbf{1_o}^{2+}$ (Figure 2a, red line) recorded at a vitreous-carbon working electrode (0.1 mM, ν = 100 mV/s) features a monoelectronic and irreversible wave at E_{pc} = −1.31 V, corresponding to the formation of $\mathbf{1_o}^{+\bullet}$. The number of electrons involved in this process, previously reported by Lehn,[26] was confirmed by comparison with the intensity of the oxidation

wave of ferrocene used as an internal standard (figure S7). During the reverse scan, an anodic signal at E_{pa} = –0.55 V is observed, corresponding to the oxidation of a substantial amount of the closed isomer $\mathbf{1}_c^{+\bullet}$.[13,26] Indeed, it was demonstrated that the electrogenerated $\mathbf{1}_o^{+\bullet}$ can be rapidly converted *in situ* at the electrode interface to its corresponding closed isomer $\mathbf{1}_c^{+\bullet}$ (Scheme 2).[24]

Further analyses revealed that the peak current ratio between the reduction of $\mathbf{1}_o^{2+}$ and the oxidation of $\mathbf{1}_c^{+\bullet}$ is neither affected by the time scale of the measurement (10 mV/s < ν < 1000 mV/s) nor by the concentration of the sample (0.01 mM < $|\mathbf{1}_o^{2+}|$ < 0.1 mM) (see Figure S5 and S6).

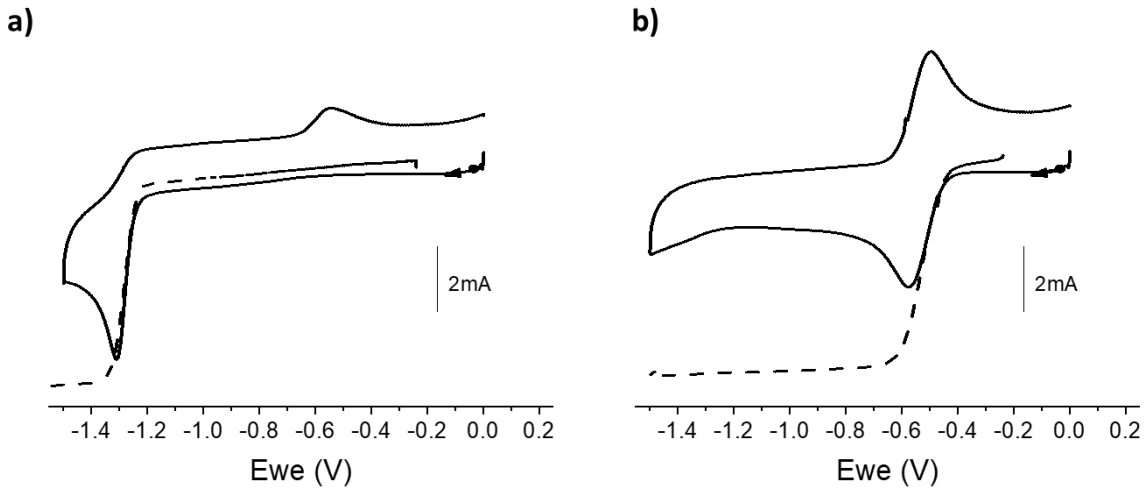

Figure 2. CV curves (full lines) and linear sweep voltammograms (rotating disk electrode (RDE), dashed lines) recorded for $\mathbf{1}_o^{2+}$ (a) and $\mathbf{1}_c^{2+}$ (b). [C]= 0.1 mM in 0.1 M TBAP/CH_3CN, Ø = 3 mm, *E* (V) *vs*. Ag^+/Ag 10^{-2} M. CV curves: ν = 100 $mV.s^{-1}$; RDE experiments: 3 mm, 600 rpm, ν = 2 mV/s of $\mathbf{1}_o^{2+}$.

This behavior can be thus summarized by the following the scheme :

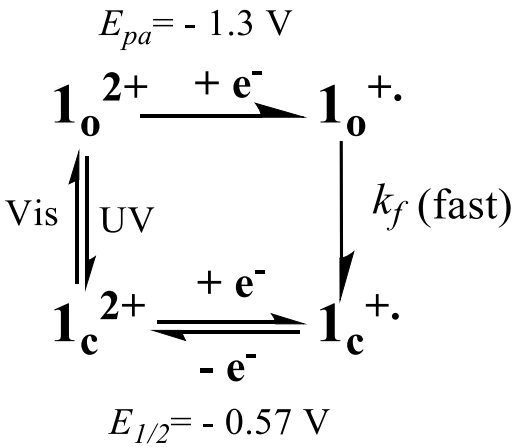

Scheme 2 : photo- and redox behavior of $\mathbf{1_o}^{2+}$

Similar studies were then carried out on the closed isomer $\mathbf{1_c}^{2+}$, produced quantitatively by continuous irradiation at 366 nm of an electrolytic solution of $\mathbf{1_o}^{2+}$ (10 mL at 0.1 mM in CH_3CN). As can be seen in Figure 2, the CV curve of $\mathbf{1_c}^{2+}$ (black line) features a one-electron reversible reduction wave (as established using ferrocene as an internal standard, see figure S7) at $E_{1/2}$ = –0.57 V (ΔE_p = 80 mV) which fits well with data reported in the literature.[13,26,36] However this result stand in sharp contrast with the electrochemical behavior of others DTE pyridinium derivatives reported in the literature, as dithiazolylethenes,[11,14] which show two reversible reduction waves attributed to the successive formation of mono- ($DTE^{\bullet-}$) and doubly-reduced (DTE^{2-}) derivatives.[14,25] Similarly, two electron-reduction waves were seen for the open and closed isomers of DTEs bearing strongly electron-withdrawing substituents such as benzonitrile.[25]

In light of these quite different observations and conclusions, we were keen to thoroughly investigate and provide a clear-cut attribution of the chemical steps coupled to the one-electron reduction observed of $\mathbf{1_c}^{2+}$.

Bulk electrolysis and spectroelectrochemical experiments

The redox behavior of $\mathbf{1}_c^{2+}/\mathbf{1}_o^{2+}$ couple have been further examined by bulk electrolysis and spectroelectrochemical experiments. Interestingly, the reduction wave of $\mathbf{1}_c^{2+}$ observed by cyclic voltammetry was found to be monoelectronic, whereas the exhaustive reduction of a solution of $\mathbf{1}_c^{2+}$ (0.1 mM in CH_3CN) carried out under dark conditions at E_{app} = –0.7 V consumed 1.5 electron per molecule. Such difference can be explained by the different timescale between cyclic voltammetry experiments and bulk electrolysis, suggesting a multistep mechanism, and will be discussed further.

In order to investigate the nature of the involved reactions, *in situ* absorption spectra were recorded over time during the electrolysis and selected UV-vis absorption spectra are displayed in Figure 3. Upon consumption of one electron per $\mathbf{1}_c^{2+}$ molecule, a blue solution attributed to the presence of $\mathbf{1}_c^{+\bullet}$ was obtained and its corresponding absorption curve displayed an intense absorption band at λ_{max} = 966 nm, associated to three less intense bands growing in the 550-800 nm region (Fig. 3a). In addition, the EPR spectrum of this solution (Figure 4) displays an intense signal at g = 2.0006 consistent with the formation of the organic radical $\mathbf{1}_c^{+\bullet}$.

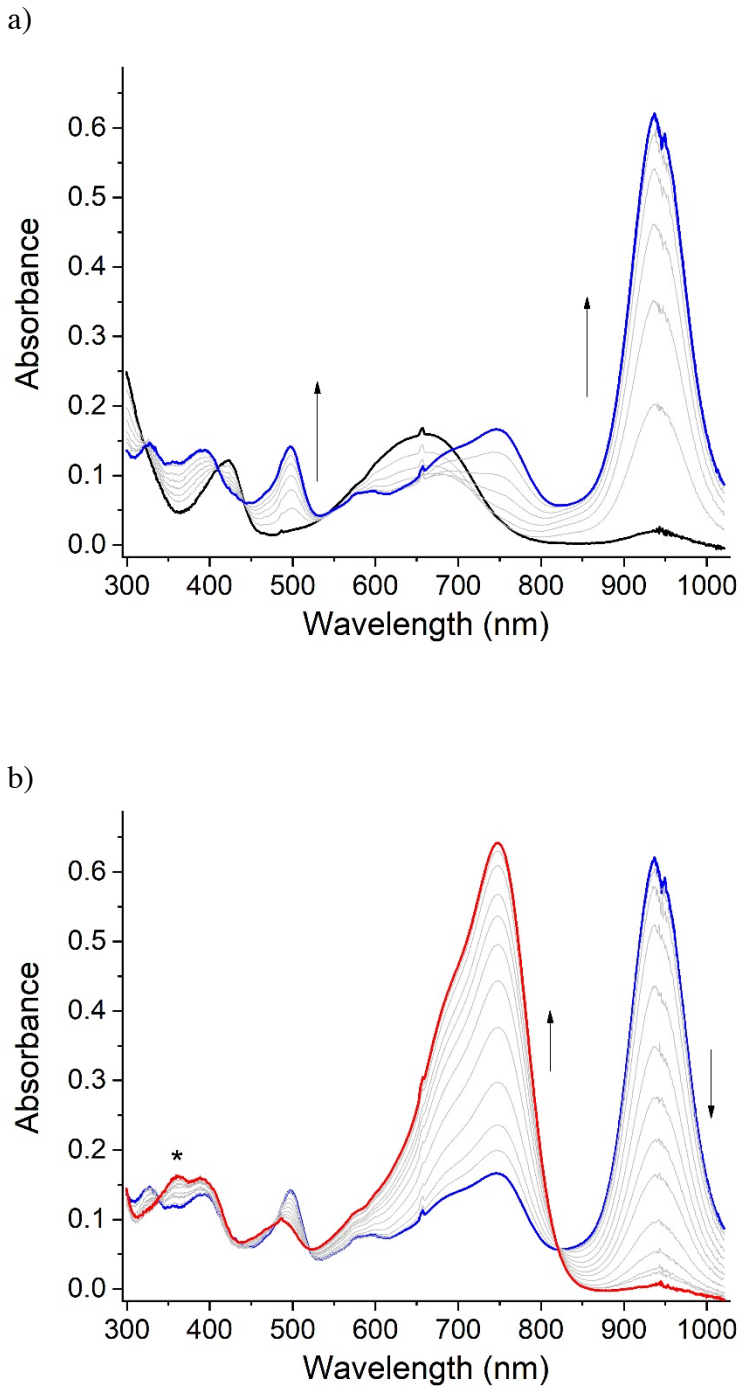

Figure 3. Evolution of the UV-vis absorption spectra during the exhaustive reduction of $\mathbf{1}_c^{2+}$ at E_{app} = –0.7V (CH_3CN + 0.1 M TBAP, 10 mL [C]= 0.1 mM); a) Evolution from 0 to 1 Faraday per

mol, b) from 1 to 1.5 faraday per mol. $\mathbf{1}_c^{2+}$ (black line), $\mathbf{1}_c^{+\bullet}$ (blue line) and $\mathbf{1}_c^{0}$ (red line). *: The band at 356 nm is attributed to the presence of $\mathbf{1}_o^{2+}$.

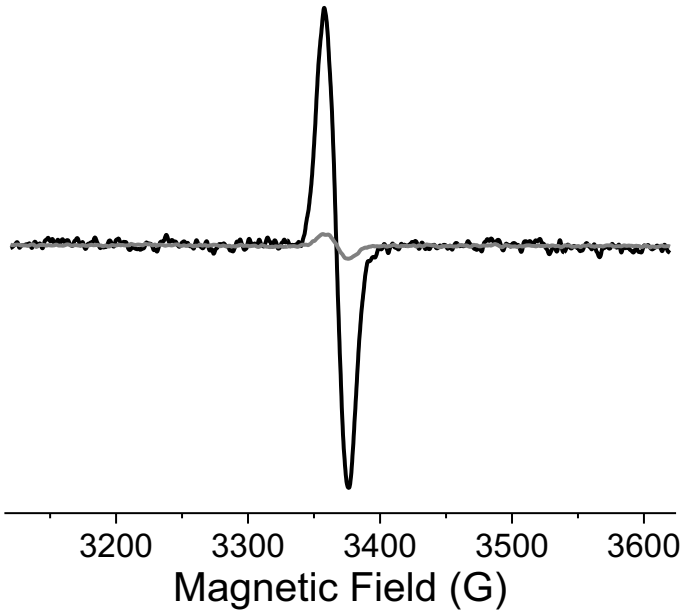

Figure 4. EPR spectra recorded at 100 K (X-band) during the electrolysis of $\mathbf{1}_c^{2+}$ (([C]= 0.1 mM in 0.1 M TBAP/CH_3CN) at E_{app} = –0.7 V (black line): intermediate state collected after addition of 1 electron *per* DTE unit; (gray line): final state obtained after addition of 1.5 Faraday *per* DTE unit.

When the electrolysis was continued (between 1 and 1.5 electron per DTE molecule), the blue solution became blue-green and a progressive disappearance of the absorption bands attributed to $\mathbf{1}_c^{+\bullet}$ (grey line in Figure 3) at the expense of new peaks growing at λ_{max} = 745 nm and 356 nm were observed, indicating the formation of a new species. EPR measurements conducted on the final

solution obtained after completion of the electrolysis, when a charge of 1.5 Coulombs per mole of DTE was obtained, resulted in the observation of a very weak signal at g =2.0006 attributed to residual traces of $\mathbf{1}_c^{+\bullet}$ (Figure 4). At this stage, based on these EPR and UV data coupled to CV experiments, our hypothesis was that the neutral diamagnetic species $\mathbf{1}_c^{0}$ could be the major product formed upon the exhaustive electrochemical reduction of $\mathbf{1}_c^{2+}$.

Theoretical calculations

In order to confirm the previous hypothesis, theoretical calculations were realized. Our computational studies aimed at optimizing the structures and assessing the relative energies of the one-electron ($\mathbf{1}_o^{+\bullet}$ and $\mathbf{1}_c^{+\bullet}$) and two-electron ($\mathbf{1}_o^{0}$ and $\mathbf{1}_c^{0}$) reduced species as well as simulating their respective absorption spectra using TD-DFT. Transition states were also computed to evaluate the activation energies associated to the isomerization (open $\leftrightarrow$ closed) of each redox state (+2, +1, 0). Some key figures related to these calculations are collected in Tables 1 and 2. First of all, we found that $\mathbf{1}_c^{+\bullet}$ lies lower in energy than $\mathbf{1}_o^{+\bullet}$ by 14.5 kcal/mol, meaning that the ring-closing reaction (open $\rightarrow$ closed) is thermodynamically favored for the mono-reduced state (ΔG_r = –12 kcal/mol). in addition, the activation energies associated to the thermal ring-closing and ring-opening reactions of the radical $\mathbf{1}^{+\bullet}$ were estimated at 14.0 and 26.0 kcal/mol, respectively. $\mathbf{1}_c^{0}$ was also found to be more stable than $\mathbf{1}_o^{0}$ by 18.3 kcal/mol, for which a biradical structure is predicted (Table S2). Therefore, in the two-electron reduced state (neutral form), the cyclization reaction is also thermodynamically favored (ΔG_r = –14.6 kcal/mol). Finally, the activation energies corresponding to the thermal ring-closing and ring-opening reactions of $\mathbf{1}^{0}$ were estimated to 12.7 and 27.3 kcal/mol. These computational results are thus fully consistent with the experimental observations discussed above and with the conclusion that the reduction of $\mathbf{1}_c^{2+}$

cannot lead to the open forms $\mathbf{1_o^{+\bullet}}$ or $\mathbf{1_o}$. They also fully support the electrochemically-triggered cyclization of $\mathbf{1_o^{2+}}$ proposed by Branda[24] and by this work.

Our interpretations of the spectroscopic data depicted in Figure 3 were then corroborated by TD-DFT calculations. The simulated absorption spectrum of $\mathbf{1_c^{+\bullet}}$ (Figure S3) shows a broad absorption band (SOMO→LUMO transition) covering the red region and extending to the near infrared region (NIR), with a maximum intensity at 848 nm falling in the same range as that observed in the experimental spectra recorded upon reduction of $\mathbf{1_c^{2+}}$ (λ_{max} = 965 nm). It should be noted that the difference of about 0.18 eV observed between the theoretical and experimental data falls within the expected accuracy of TD-DFT (within 0.25 eV for valence states).[37] A few more, less intense, absorption bands are also predicted to be observed between 350-500 nm. In contrast, the calculated spectrum of $\mathbf{1_c^{0}}$ does not exhibit any absorption band in the NIR region (Figure S4), which supports our conclusion that the band at 965 nm is a diagnostic signature of $\mathbf{1_c^{+\bullet}}$. On the other hand, the calculated spectrum of $\mathbf{1_c^{0}}$ features a broad and intense absorption band centered at 650 nm which matches quite well with the absorption signal observed between 700 and 750 nm in the experimental spectrum (again within the 0.25 eV margin of error).

To sum up, the good match observed between TD-DFT calculations and experimental data supports the attribution and conclusions raised above on the ground of experimental data. In particular, both studies reveal a strong red-shift of the absorption bands when going from the dicationic species $\mathbf{1_c^{2+}}$ to the radical cation $\mathbf{1_c^{+\bullet}}$, and a blue-shift when converting the radical cation into its corresponding neutral species $\mathbf{1_c^{0}}$ (Table 1). These attributions are also in full agreement with previous studies carried out on a pyridinium-substituted dithiazolylethene[14] showing that the UV-vis absorption spectra of the cation radical and neutral products, obtained after successive

reduction of 1 and 2 electrons per mole respectively, are similar to those collected throughout the exhaustive reduction of $\mathbf{1_c^{2+}}$.

Table 1. Lowest vertical electronic transitions computed at the TD-DFT level in acetonitrile for compound **1** in different redox states. Experimental wavelengths are compared to theoretical values. (Experimental conditions: CH_3CN (10 ml, l = 10 mm, c=0.1 mM)

Compounds	λ_{max}^{expt} (nm)	ε^{expt} (10^3 $cm^{-1}M^{-1}$)	ΔE^{calc} (kcal/mol)	λ^{calc} (nm)	f [a]	Transitions [b]
$\mathbf{1_o^{2+}}$	356	45	79.7	359	1.002	H→L
$\mathbf{1_c^{2+}}$	669	14	41.7	685	0.462	H→L
			60.4	473	0.034	H→L+1
	426	9	64.9	440	0.134	H–1→L
$\mathbf{1_c^{+\bullet}}$			20.5	1392	0.064	H–1→S
	965	38	33.7	848	0.976	S→L
$\mathbf{1_c^{0}}$	746	54	44.2	647	1.327	H→L

[a] Oscillator strengths. [b] Main configurations (H: HOMO, L: LUMO, S: SOMO). Main contributing orbitals shown in Figures S1–S4).

Table 2. Computed reaction energies (ΔE_r), Gibbs free reaction energies (ΔG_r) potential energy barriers ($\Delta E^{\ddagger}$) and activation energies ($\Delta G^{\ddagger}$) in acetonitrile.

Reactions	ΔE_r (kcal/mol)	ΔG_r (kcal/mol)	$\Delta E^{\ddagger}$ (kcal/mol)	$\Delta G^{\ddagger}$ (kcal/mol)
$\mathbf{1_o^{2+} \rightarrow 1_c^{2+}}$	18.1	20.6	41.9	42.8
$\mathbf{1_o^{+} \rightarrow 1_c^{+\bullet}}$	–14.5	–12.0	12.8	14.0
$\mathbf{1_o \rightarrow 1_c^{0}}$	–18.3	–14.6	12.2	12.7

Study of the stability of the electrogenerated compounds

The voltammetric curve collected at a Rotating Disk Electrode (RDE) after completion of the exhaustive reduction at E_{app} = –0.7 V (Figure 5), *i.e.* after addition of 1.5 F/mol revealed the presence in the mixture of ~80 % of the fully reduced compound $\mathbf{1_c^{0}}$ (which is oxidized at E ~ –0.5 V) together with ~15% of an open isomer (which is reduced at E ~ –1.4 V and exhibits an

absorption band at 356 nm)) and less than 10% of a third unknown product (which is oxidized at $E \sim -0.75$ V ; * in Figure 5).

The reversibility of the redox processes involved in solution was investigated by re-oxidation of the mixture previously obtained after exhaustive reduction of $\mathbf{1}_c^{2+}$ at $E_{app} = -0.7$ V. This was achieved upon setting the potential of the working electrode at $E_{app} = -0.3$ V. During electrolysis, a progressive decrease in intensity of the absorption band at 745 nm (corresponding to $\mathbf{1}_c^{0}$) was observed and new signals increased first at 966 nm and then at 668 nm, attributed to the formation of $\mathbf{1}_c^{+\bullet}$ and $\mathbf{1}_c^{2+}$, respectively (Figure S8). RDE data collected after completion of the re-oxidation (red dashed line in figure 5) surprisingly revealed a significant increase in the relative concentration of both the open isomer and the side product. This behavior was further confirmed since repeated reduction/oxidation cycles led to a progressive accumulation of those two species in solution (see figure S9).

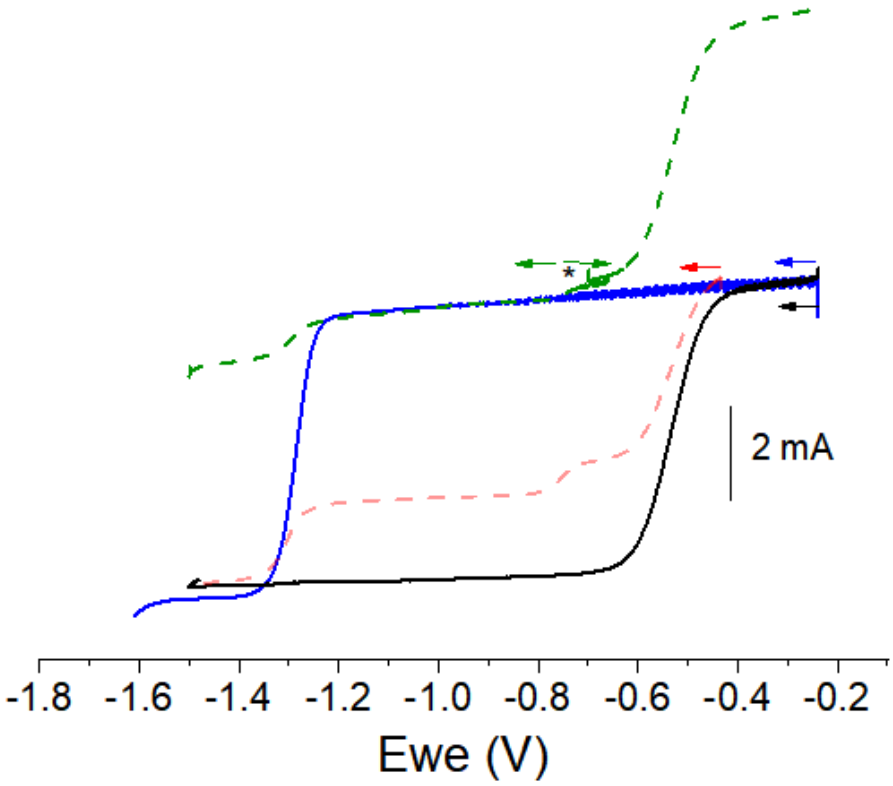

Figure 5. Linear sweep voltammograms at 2 mV/s of: $\mathbf{1}_o^{2+}$ (blue), $\mathbf{1}_c^{2+}$ (black, solution A), solution A reduced with 1.5 F/mol (solution B, dotted green) and solution B upon oxidation at E_{app} = –0.3 V (red curve), RDE experiments: GC, 3 mm, 600 rpm, ν = 2 mV/s

These results led us to question the stability of the *in-situ* generated species $\mathbf{1}_c^{\bullet+}$ and $\mathbf{1}_c^{0}$ over time (exhaustive electrolysis at E_{app} = –0.7 V) The evolution of the solutions was investigated by periodic recordings (over a total period of 24 hours and without polarization) of the spectroscopic and electrochemical signatures of a solution of $\mathbf{1}_c^{\bullet+}$ or $\mathbf{1}_c^{0}$ (Figure 6). In the case of $\mathbf{1}_c^{\bullet+}$, UV-visible spectrum of the solution clearly evolves in a first time to the formation of $\mathbf{1}_c^{0}$ (see figure S12) as observed by the disappearance of the band located at 966 nm and the increase of the band located

at 750 nm attributed to the $\mathbf{1_c^0}$ form (see figure S12). This evolution can be explained by the disproportionation process:

$$\mathbf{1}_c^{+\cdot} + \mathbf{1}_c^{+\cdot} \rightleftharpoons \mathbf{1}_c^{2+} + \mathbf{1_c^0}$$

Then, this solution continues to change with time (see Fig. S12) until an unknown product is formed, with an absorption band at 750nm. In order to identify this latest compound, the spectroscopic and electrochemical evolutions of a fresh solution of $\mathbf{1_c^0}$ were followed (Figure 6). At the beginning of the experiment, a reversible oxidation wave centered at $E_{1/2}$= –0.57 V was observed by cyclic voltammetry and an intense absorption band centered at 750 nm was measured. As can be seen in Figure 6a and 6b, the intensities of these initial redox and UV-vis signals were found to gradually decrease over time in favor of a new reversible wave centered at –0.75 V and of another absorption band centered at 750 nm, both of them being attributed to the same side product initially considered on the ground of the electrolysis data depicted in Figure 5.

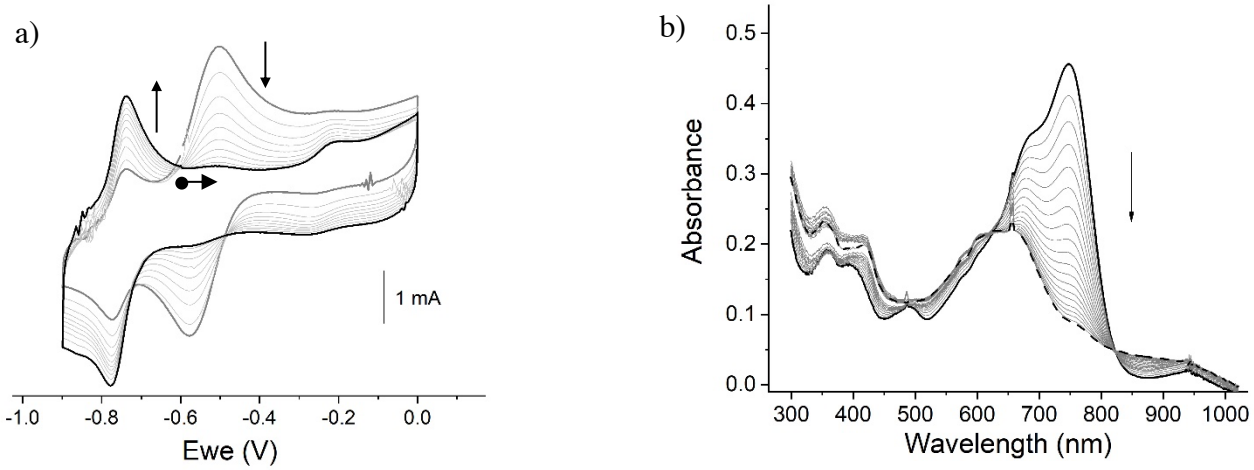

Figure 6. Evolution of the CV (a) and UV-vis (b) spectra recorded during 24h (step 2h in absence of polarization except when CV is recorded) on the *in situ* generated $\mathbf{1_c^0}$ (exhaustive electrolysis at E_{app} = –0.7 V, CH_3CN + 0.1 M TBAP, [C]= 0.1 mM).

In order to determine the nature of this unknown product, this former was produced at larger scale by reaction of $\mathbf{1}_c^{2+}$ in acetonitrile with 1.5 equivalents of cobaltocene used as chemical reductant ($E_{1/2}$ = −1.2 V). The resulting solution was then stirred in the dark at room temperature for 2 days and the mixture was ultimately separated and purified by column chromatography column on SiO_2. The most abundant blue-colored product could be crystallized (by slow diffusion of diethyl ether in CH_3CN) and characterized by X-ray diffraction. The solid-state structure depicted in Figure 7 shows that this monocationic product (named **7-DTE**) incorporates only one pyridinium ring and one neutral quinoid-like pyridine. Two fluorine atoms of the central cyclopentene ring have also been replaced by a carbonyl moiety. The four heterocycles are coplanar, separated by a seven-membered ring which introduces a kink. The overall planar conformation results from an efficient pi-conjugation extended on one side from the quinoid-like pyridine to the ketone, and on the other side from the electron-deficient pyridinium to the electron-rich thiophene.

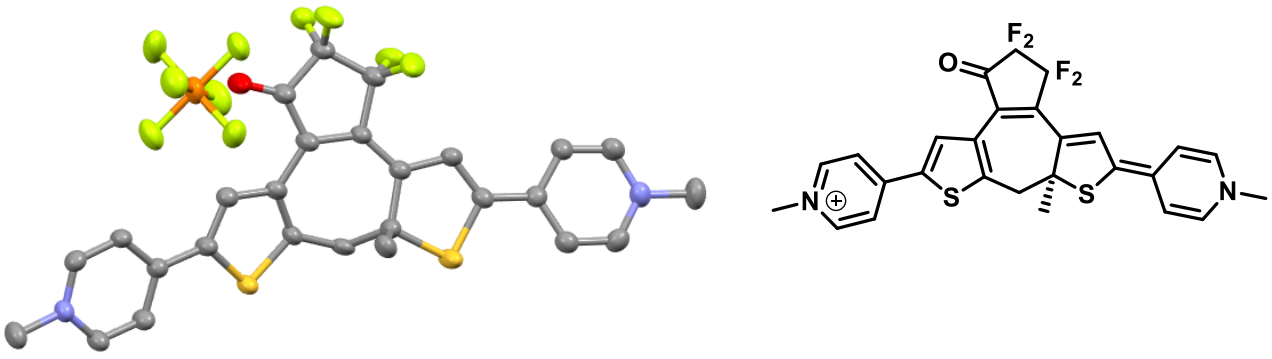

Figure 7. X-ray structure (left) and schematic representation (right) of the reaction product **7-DTE**. Ellipsoids are set at a 50% probability; hydrogen atoms have been omitted for clarity purposes.

The formation of seven-membered ring from other DTE derivatives has already been reported in the literature by Hecht[38] and Huhn.[39] In both cases the proposed mechanism is initiated by deprotonation of one internal methyl substituent yielding a nucleophilic carbanion which reacts with the adjacent thiophene. In the present study, the spectroelectrochemical behavior of $\mathbf{1}_c^{2+}$ in the presence of a base was followed and such deprotonation could be rejected. Indeed, absorption spectra recorded over time during the potentiostatic reduction of $\mathbf{1}_c^{2+}$ at $E_{app} = -0.7$ V in the presence of an excess of NaOH or lutidine (10 eq in CH_3CN) gave identical results to those previously collected in the absence of base (exchanged charge, spectroscopic data).

Another possible route for the formation of **7-DTE** from $\mathbf{1}_c^{0}$ is represented in Scheme 3. It starts with the release of a hydride anion and the formation of $\mathbf{2}_c^{+}$ which is spontaneously opened to its corresponding $\mathbf{2}_o^{+}$ isomer. This is then followed by an intramolecular ring-closure reaction proceeding through an intramolecular electrophilic aromatic addition of the carbenium onto the electron-rich thiophene to afford $\mathbf{3}_c^{+}$. DFT calculations confirm these hypotheses. Indeed, the closed-form intermediates $\mathbf{2}_c^{+}$ can evolve into the more stable open isomer $\mathbf{2}_o^{+}$, lying 10 kcal/mol lower in energy. The ring-closure reaction, corresponding to the formation $\mathbf{3}_c^{+}$ is also energetically favorable as well, $\mathbf{3}_c^{+}$ being 19 kcal/mol lower in energy than $\mathbf{2}_c^{+}$.

The last step corresponds to the formation of **7-DHP** obtained by oxidation of a CF_2 fragment in $\mathbf{3}_c^{+}$ into a ketone. We believe that this reaction was realized during the purification process. Indeed, when trying to isolate $\mathbf{3}_c^{+}$ by column chromatography, this compound was found to be unstable since a color change was clearly observed. This color change was attributed to the spontaneous formation of **7-DTE** under aerobic conditions and/of in the presence of water.

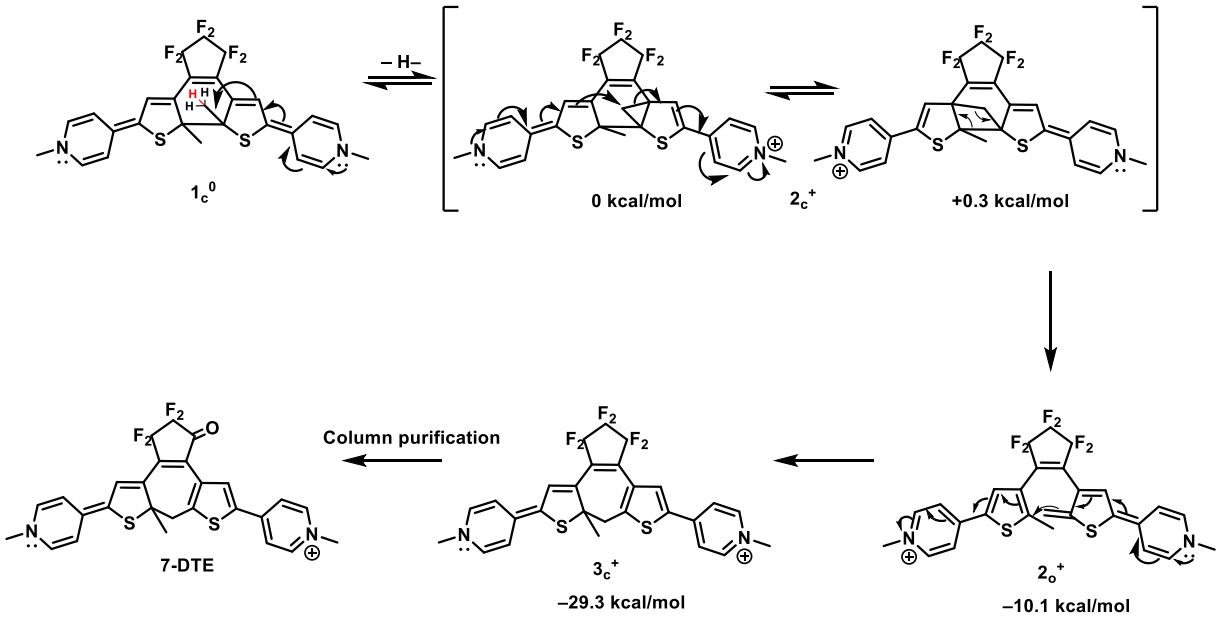

Scheme 3. Proposed mechanism for the formation of the seven-membered ring derivative **7-DTE** form $\mathbf{1_c^0}$.

In addition, the overall electrochemical mechanism, starting form a solution of $\mathbf{1c^{2+}}$, can be represented by the following redox and chemical equations (1-5):

$$2^{*}\mathbf{1}_c^{2+} + 2e^- \longrightarrow 2^{*}\mathbf{1}_c^{+\cdot} \qquad (1)$$

$$\mathbf{1}_c^{+\cdot} + \mathbf{1}_c^{+\cdot} \rightleftharpoons \mathbf{1}_c^{2+} + \mathbf{1}_c^{0} \qquad (2)$$

$$\mathbf{1}_c^{0} \longrightarrow \mathbf{3}_c^{+} + H^- \qquad (3)$$

$$\mathbf{1}_c^{2+} + 1e^- \longrightarrow \mathbf{1}_c^{+\cdot} \qquad (4)$$

$$\mathbf{1}_c^{+\cdot} + H^- \longrightarrow \mathbf{1}_c^{0} + 1/2H_2 \qquad (5)$$

$$2^{*}\mathbf{1}_c^{2+} + 3e^- \longrightarrow 2^{*}\mathbf{3}_c^{+} + 1/2H_2$$

Upon reduction of $\mathbf{1_c^{2+}}$ to $\mathbf{1_c^{+\bullet}}$ (eq. 1), $\mathbf{1_c^{2+}}$ and $\mathbf{1_c^{0}}$ compounds are produced by a disproportionation step (eq. 2). $\mathbf{1_c^{0}}$ then evolves towards $\mathbf{3_c^{+}}$ (and then **7-DHP**, following the mechanism represented in Scheme 3) which is accompanied by the release of a hydride anion per molecule (eq. 3). The $\mathbf{1_c^{2+}}$ derivative, previously regenerated in eq. 2 is then reduced at the electrode to afford $\mathbf{1_c^{+\bullet}}$ (eq. 4) and then 1c+• can be chemically reduced in to the presence of H^- (eq. 5). Thus, the overall mechanism corresponds the electrochemical reduction of $\mathbf{1_c^{2+}}$ by 1.5 Coulomb per mole, as observed experimentally when $\mathbf{1_c^{2+}}$ is electrolysed at E_{app} = –0.7 V.

In order to further confirm these reactions, the electrolysis of $\mathbf{1_c^{2+}}$ was realized in the presence of $B(C_6F_5)_3$ as a hydride abstracting agent. For this experiment, a mixture of $B(C_6F_5)_3$ (0.1 mM) and $\mathbf{1_c^{2+}}$ (0.1 mM) in acetonitrile were submitted to an exhaustive reduction at E_{app} = –0.7 V. The UV-vis spectrum recorded for the blue solution obtained after addition of one electron/molecule of $\mathbf{1_c^{2+}}$ exhibits an intense absorption band centered at 966 nm and a less intense one at 675 nm. Further reduction of the solution, until the addition of two electrons/mole, led to the progressive disappearance of the band at 966 nm attributed to $\mathbf{1_c^{+\bullet}}$ for the benefit of a band at λ_{max} = 745 nm assigned to the doubly reduced species $\mathbf{1_c^{0}}$ (see figure S10). At the end of the electrolysis, 2F/Mole of $\mathbf{1_c^{2+}}$ were consumed (as expected for the production of $\mathbf{1_c^{0}}$ from $\mathbf{1_c^{2+}}$), in contrast with the 1.5F/mol experimentally obtained in the absence of $B(C_6F_5)_3$. This experiment corroborates our hypothesis that H^- is released in the solution from $\mathbf{1_c^{0}}$ (eq. 3). Indeed, in the presence of $B(C_6F_5)_3$, H- is consumed and cannot plays the role of chemical reductant in eq. 5 and 2 electrons per $\mathbf{1_c^{2+}}$ molecules are thus needed.

We also found that the cyclic voltammogram recorded after completing the two-electron reduction of $\mathbf{1_c^{2+}}$ in the presence of $B(C_6F_5)_3$ exhibits two reversible waves at –0.5 and –0.75 V assigned to

the oxidation of $\mathbf{1_c^0}$ and to the reduction of the intermediate compound, $\mathbf{3_c^+}$, respectively (see figure S11). In agreement with our preliminary experiments demonstrating the limited stability of $\mathbf{1_c^0}$, we also found that the electrochemical signature of the mixture evolves over time towards a unique signal at $E_{1/2}$ = –0.75 V attributed to the reversible reduction of $\mathbf{3_c^+}$.

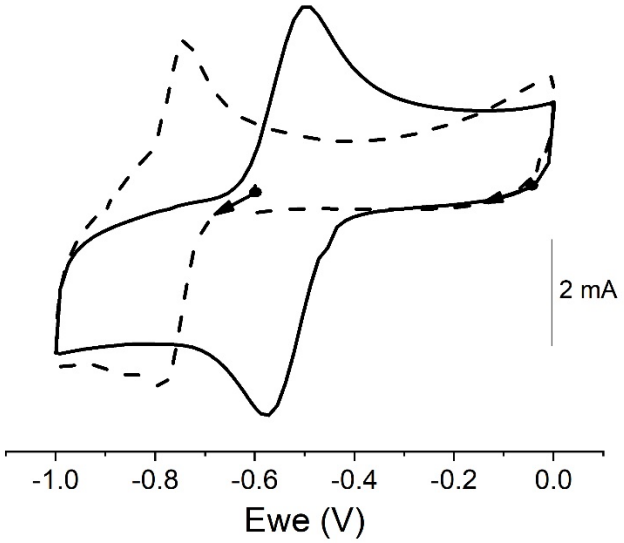

Figure 8. CV curves recorded for a freshly prepared solution of the $\mathbf{1_c^{2+}}$ (CH_3CN + 0.1 M TBAP, [C]= 0.1 mM) (full line), and after 2 days of stirring in presence of $B(C_6F_5)_3$ (0.1 mM in CH_3CN) (dashed line).

The electrochemical behavior and the absorption spectrum of the isolated closed-ring species **7-DHP** , are depicted in figure 9 (data of $\mathbf{3_c^+}$ are also shown for comparison). The 7**-DHP** system undergoes two successive one-electron oxidation signals. The first reversible oxidation wave is observed at $E_{1/2}$ = 0 V whereas the second irreversible peak is observed at Ep_a= + 0.62 V. The corresponding absorption spectrum, recorded in the 300 nm–900 nm range, displays two main

bands at 670 and 359 nm attributed to the π–π* transitions of the chromophore. These absorption bands appear bathochromically shifted in the ketone derivative comparing to the parent $\mathbf{3_c^+}$.

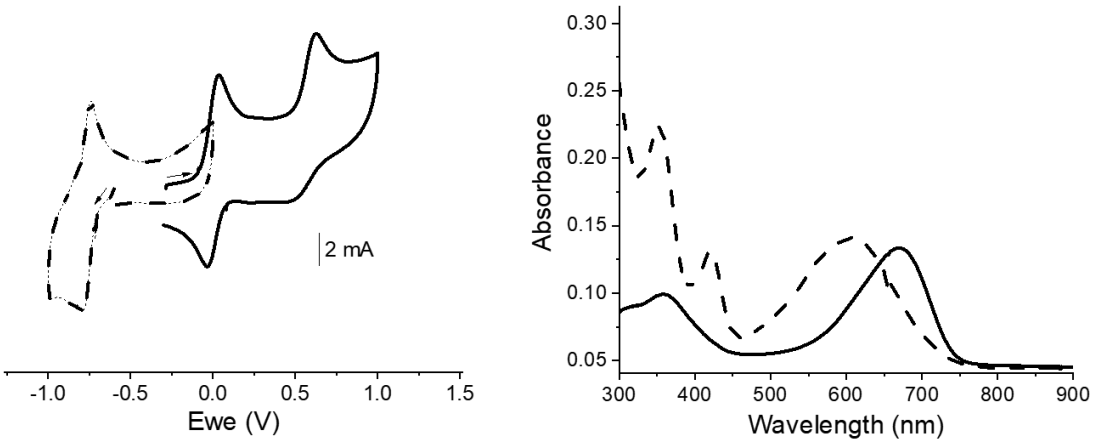

Figure 9. CV spectra and UV-vis absorption spectra of **7-DHP** (full line) and $\mathbf{3_c^+}$ (dashed line) in CH_3CN + 0.1 M TBAP. [C]= 0.1 mM.

Conclusions

The optical and redox properties of a methyl pyridinium appended 1,2-dithienylethene derivative $\mathbf{1_c^{2+}}$ were deeply investigated. Spectro-electrochemical studies coupled with EPR spectroscopy and theoretical calculations clearly indicate that reduction of the closed isomer $\mathbf{1_c^{2+}}$ to $\mathbf{1_c^0}$ is performed through a two-step mechanism involving the radical cation $\mathbf{1_c^{+\bullet}}$ as an intermediate. It has been pointed out that the reduced $\mathbf{1_c^0}$ form is not stable with time and it can undergo a H^- abstraction followed by an arrangement towards a seven-membered ring species **7-DHP**. The $\mathbf{1_c^{2+}/1_o^{2+}}$ couple, which can follow multiple redox- and optically-triggered ring-opening and closing reactions, represents thus a very attractive system in particular for applications in molecular electronics.

ASSOCIATED CONTENT

Supporting Information. Additional procedures and methods, computational details, computed absorption spectra, additional UV-vis spectra, computed structures

The following files are available free of charge.

AUTHOR INFORMATION

Corresponding Author

*saioa.cobo@univ-grenoble-alpes.fr

Author Contributions

The manuscript was written through contributions of all authors. All authors have given approval to the final version of the manuscript.

ACKNOWLEDGMENT

The authors wish to acknowledge the support of the Institut Universitaire de France.

REFERENCES

[1] W. R. Feringa, B. L., & Browne, Ed. , *Molecular Switches*, **2011**.

[2] A. Bakkar, F. Lafolet, D. Roldan, E. Puyoo, D. Jouvenot, G. Royal, E. Saint-Aman, S. Cobo, *Nanoscale* **2018**, *10*, 5436–5441.

[3] M. Jacquet, L. M. Uriarte, F. Lafolet, M. Boggio-Pasqua, M. Sliwa, F. Loiseau, E. Saint-Aman, S. Cobo, G. Royal, *J. Phys. Chem. Lett.* **n.d.**, *11*, 2682–2688.

[4] M. Irie, T. Fukaminato, K. Matsuda, S. Kobatake, *Chem. Rev.* **2014**, *114*, 12174–12277.

[5] S. Kobatake, S. Takami, H. Muto, T. Ishikawa, M. Irie, *Nature* **2007**, *446*, 778–81.

[6] T. Fukaminato, T. Hirose, T. Doi, M. Hazama, K. Matsuda, M. Irie, *J. Am. Chem. Soc.* **2014**, *136*, 17145–17154.

[7] A. Peters, N. R. Branda, S. Fraser, V. Uni, V. Uni, V. Dri, C. Va, *J. Am. Chem. Soc.* **2003**, *125*, 3404–3405.

[8] S. Cobo, A. Khettabi, A. Grempka, F. Lafolet, E. Chatir, N. Leconte, M.-N. Collomb, D. Jouvenot, *Chem. - A Eur. J.* **2020**, *26*, 13359–13362.

[9] S. Muratsugu, S. Kume, H. Nishihara, *J. Am. Chem. Soc.* **2008**, *130*, 7204–7205.

[10] R. H. Mitchell, Z. Brkic, V. A. Sauro, D. J. Berg, *J. Am. Chem. Soc.* **2003**, *125*, 7581–7585.

[11] N. Baggi, A. Léaustic, S. Groni, E. Anxolabéhère-Mallart, R. Guillot, R. Métivier, P. Yu, *Chem. - A Eur. J.* **2021**, *27*, 12866–12876.

[12] G. Guirado, C. Coudret, M. Hliwa, J. Launay, *J. Phys. Chem. B* **2005**, *109*, 17445–17459.

[13] B. Gorodetsky, H. D. Samachetty, R. L. Donkers, M. S. Workentin, N. R. Branda, *Angew. Chem. Int. Ed.* **2004**, *43*, 2812–2815.

[14] A. Léaustic, E. Anxolabéhère-Mallart, F. Maurel, S. Midelton, R. Guillot, R. Métivier, K. Nakatani, P. Yu, *Chem. - A Eur. J.* **2011**, *17*, 2246–2255.

[15] T. Koshido, T. Kawai, K. Yoshino, *J. Phys. Chem.* **1995**, *99*, 6110–6114.

[16] T. Nakashima, Y. Kajiki, S. Fukumoto, M. Taguchi, S. Nagao, S. Hirota, T. Kawai, *J. Am. Chem. Soc.* **2012**, *134*, 19877–19883.

[17] S. Lee, Y. You, K. Ohkubo, S. Fukuzumi, W. Nam, *Chem. Sci.* **2014**, *5*, 1463–1474.

[18] J. P. Calupitan, T. Nakashima, Y. Hashimoto, T. Kawai, *Chem. - A Eur. J.* **2016**, *22*, 10002–10008.

[19] A. Peters, N. R. Branda, *Chem. Commun.* **2003**, 954–955.

[20] W. R. Browne, J. J. D. De Jong, T. Kudernac, M. Walko, L. N. Lucas, K. Uchida, J. H. Van Esch, B. L. Feringa, *Chem. - A Eur. J.* **2005**, *11*, 6414–6429.

[21] W. R. Browne, J. J. D. De Jong, T. Kudernac, M. Walko, L. N. Lucas, K. Uchida, J. H. Van Esch, B. L. Feringa, *Chem. - A Eur. J.* **2005**, *11*, 6430–6441.

[22] B. He, O. S. Wenger, *J. Am. Chem. Soc.* **2011**, *133*, 17027–17036.

[23] Y. Moriyama, K. Matsuda, N. Tanifuji, S. Irie, M. Irie, *Org. Lett.* **2005**, *7*, 3315–3318.

[24] B. Gorodetsky, N. R. Branda, *Adv. Funct. Mater.* **2007**, *17*, 786–796.

[25] M. Kleinwächter, E. Teichmann, L. Grubert, M. Herder, S. Hecht, *Beilstein J. Org. Chem.* **2018**, *14*, 2812–2821.

[26] S. L. Gilat, S. H. Kawai, J. -M Lehn, *Chem. – A Eur. J.* **1995**, *1*, 275–284.

[27] K. Yamaguchi, F. Jensen, A. Dorigo, K. N. Houk, *Chem. Phys. Lett.* **1988**, *149*, 537–542.

[28] S. Yamanaka, T. Kawakami, H. Nagao, K. Yamaguchi, *Chem. Phys. Lett.* **1994**, *231*, 25–

33.

[29] J. Da Chai, M. Head-Gordon, *Phys. Chem. Chem. Phys.* **2008**, *10*, 6615–6620.

[30] P. C. Hariharan, J. A. Pople, *Theor. Chim. Acta* **1973**, *28*, 213–222.

[31] W. J. Hehre, K. Ditchfield, J. A. Pople, *J. Chem. Phys.* **1972**, *56*, 2257–2261.

[32] C. Adamo, V. Barone, *J. Chem. Phys.* **1999**, *110*, 6158–6170.

[33] T. Clark, J. Chandrasekhar, G. W. Spitznagel, P. V. R. Schleyer, *J. Comput. Chem.* **1983**, *4*, 294–301.

[34] S. Aloïse, M. Sliwa, G. Buntinx, S. Delbaere, A. Perrier, F. Maurel, D. Jacquemin, M. Takeshita, *Phys. Chem. Chem. Phys.* **2013**, *15*, 6226–6234.

[35] M. J. Frisch, G. W. Trucks, H. B. Schlegel, G. E. Scuseria, M. A. Robb, J. R. Cheeseman, G. Scalmani, V. Barone, G. A. Petersson, H. Nakatsuji, X. Li, M. Caricato, A. Marenich, J. Bloino, B. G. Janesko, R. Gomperts, B. Mennucci, H. P. Hratchian, J. V. Ortiz, A. F. Izmaylov, J. L. Sonnenberg, D. Williams-Young, F. Ding, F. Lipparini, F. Egidi, J. Goings, B. Peng, A. Petrone, T. Henderson, D. Ranasinghe, V. G. Zakrzewski, J. Gao, N. Rega, G. Zheng, W. Liang, M. Hada, M. Ehara, K. Toyota, R. Fukuda, J. Hasegawa, M. Ishida, T. Nakajima, Y. Honda, O. Kitao, H. Nakai, T. Vreven, K. Throssell, J. A. Montgomery, Jr., J. E. Peralta, F. Ogliaro, M. Bearpark, J. J. Heyd, E. Brothers, K. N. Kudin, V. N. Staroverov, T. Keith, R. Kobayashi, J. Normand, K. Raghavachari, A. Rendell, J. C. Burant, S. S. Iyengar, J. Tomasi, M. Cossi, J. M. Millam, M. Klene, C. Adamo, R. Cammi, J. W. Ochterski, R. L. Martin, K. Morokuma, O. Farkas, J. B. Foresman, and D. J. Fox, Gaussian

09, Revision D.01, Gaussian, Inc., Wallingford CT, **2009**.

[36] J. Piard, R. Métivier, M. Giraud, A. Léaustic, P. Yu, K. Nakatani, *New J. Chem.* **2009**, *33*, 1420.

[37] A. D. Laurent, D. Jacquemin, *Int. J. Quantum Chem.* **2013**, *113*, 2019–2039.

[38] M. Herder, M. Utecht, N. Manicke, L. Grubert, M. Pätzel, P. Saalfrank, S. Hecht, *Chem. Sci.* **2013**, *4*, 1028–1040.

[39] D. Sysoiev, T. Huhn, *Photochem. Photobiol. Sci.* **2020**, *19*, 1511–1516.

Table of Contents

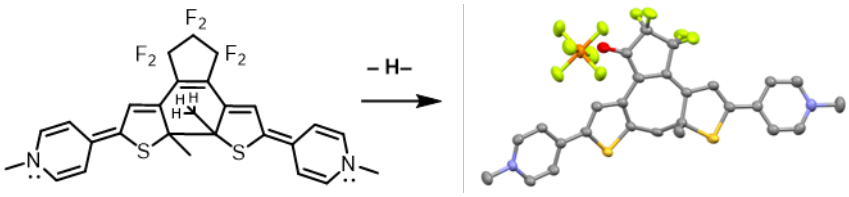

The optical and redox properties of a methyl pyridinium appended 1,2-dithienylethene photochromic derivative have been thoroughly investigated. A complex multi-step photo/redox mechanism is proposed for the closed isomer on the ground of spectro-electrochemical and theoretical data. The generated compounds are not stable over the time because of chemical reactions associated to the redox processes and a new dithienylethene derivative incorporating a seven-membered ring has been isolated and characterized.